JOURNAL OF COMPUTATIONAL PHYSICS 35, 254–283 (1980)

Numerical Codes for Cylindrical General Relativistic Systems

TSVI PIRAN

*Center for Relativity, University of Texas, Austin, Texas 78712**

Received April 17, 1979

Various numerical methods for solutions of Einstein equations are presented and discussed. The numerical schemes are classified according to the equations (evolution versus constraint) solved and according to the coordinate conditions used. The numerical methods are compared by using them to study systems with cylindrical symmetry for vacuum (Einstein–Rosen waves), matter collapse, and cosmology (perturbation of Friedmann Universe).

I. INTRODUCTION

In recent years there has been a growing interest in numerical solutions of Einsteins' equations. Many astrophysically interesting situations involve asymmetric dynamic general relativistic strong fields for which the standard analytic (perturbation) methods do not yield a solution. In particular two related questions of current great interest are the generation of gravitational waves and the gravitational collapse and formation of black holes. It is hoped that like in other branches of physics and astrophysics numerical methods could yield a solution to these questions [1].

May and White [2] have written a numerical code for a general relativistic spherically symmetric collapse. Due to the spherical symmetry of their solution the dynamical character of the general relativistic equations disappears and along with it any gravitational waves and the numerical difficulties associated with them. Epply and Smarr [3, 4] have solved numerically the problem of axisymmetric black-holes collisions and Wilson and Smarr [5–7] have calculated numerically axisymmetric perfect fluid collapse to a neutron star. In these configurations there is one mode of gravitational wave present. While the results of these calculations are very impressive and are of great astrophysical importance, there are still a number of open questions involved in numerical general relativity.

As is well known, general relativity on a lattice (numerical grid) is an overdetermined system of equations for the geometry variables. (The system is not overdetermined in the continuum case by virtue of the Bianchi identities, however these cannot be satisfied on a lattice.) This together with the usual coordinate freedom of general relativity introduce an additional arbitrariness when constructing numerical

* Present address: The Institute for Advanced Study, Princeton, NJ 08540.

0021-9991/80/050254-30$02.00/0

schemes. The equations are divided into evolution (hyperbolic) and constraint (elliptic) equations. Numerical schemes can be classified according to choices between these two types of equations. Such a classification is presented and different schemes are compared. The standard numerical freedom, the grid structure, and possible variations of the grid spacing during the numerical solution by use of grid velocity are also discussed.

In this work I study the behavior of cylindrically symmetric general relativistic numerical schemes. These are one spatial dimensional schemes, which, in contrast to the spherical configurations, do include gravitational waves. (In general two modes of gravitational waves are possible with this symmetry, but by imposing additional mirror symmetry only one mode is allowed.) These schemes are, therefore, in an intermediate stage between the spherical May and White [2] code and the two-dimensional codes of Eppley and Smarr [3, 4] and Wilson [5–7]. They can serve as an excellent arena for comparing different numerical methods and between the different arbitrary choices which were described earlier. The penalty involved in the usage of a cylindrical system is the associated difficulty with the behavior at large r (cylindrical systems are not asymptotically flat).

The general formalism and methods for numerical solutions for general relativity are discussed in the second section. This discussion is limited to methods based on the ADM (Arnowitt, Deser, and Misner) [8] formalism. The equations for a cylindrical symmetry are derived in the next section. This is followed by a detailed discussion of the numerical methods used. Results for propagation of waves in vacuum are presented and compared for various schemes. It is found that the fully constrained schemes are the best from the numerical point of view, even though it was possible to derive reasonable solutions using other methods. Finally, results of cylindrical matter collapse and of evolution of cylindrical perturbation on a Friedmann Universe are shown.

II. General Formalism

A general relativistic hydrodynamic problem involves the solution of the Einstein equations for the geometry variables together with the energy-momentum conservation equations and the equation of state for the matter variables:

$$G_{\mu\nu} = T_{\mu\nu}, \tag{1}$$

$$T_{\mu}{}^{\nu}{}_{,\nu} = 0, \tag{2}$$

$$p = p(\rho, e). \tag{3}$$

$G_{\mu\nu}$ and $T_{\mu\nu}$ are the Einstein and energy-momentum tensors and ρ, n, e, and p are the total density, baryon number density, and internal energy per baryon and pressure, respectively ($\rho = n(1 + e)$). In our units $8\pi G = c = 1$.

A numerical Cauchy problem [19] in which the values are specified on an initial hypersurface and their time evolution is calculated is best formulated using the ADM

formalism [8]. Space-time is sliced into a foliation of three-dimensional, constant t, spatial hypersurfaces, each of which are described by a three metric ${}^{(3)}g_{ij}$ ($i, j = 1, 3$; the superscript (3) will be omitted in the following discussion) and its extrinsic curvature tensor K_j^i. The foliation is determined by α, the lapse function, and the coordinate transformation between two infinitely close slices is determined by the shift vector β^i. The general line element is

$$ds^2 = -\alpha^2 dt^2 + {}^{(3)}g_{ij}(dx^i + \beta^i dt)(dx^j + \beta^j dt). \tag{4}$$

Using the identity

$$\frac{\partial}{\partial t} g_{ij} = -2\alpha g_{ik} K_j^{\ k} + \beta^k g_{ij,k} + g_{ik}\beta^k{}_{,j} + g_{jk}\beta^k{}_{,i}\,, \tag{5}$$

project Eq. (1) along $n^\mu n^\nu$, $n^\nu(\delta_i{}^\mu - n^\mu n_i)$, and $(\delta_i{}^\mu - n^\mu n_i)(\delta_j{}^\nu - n^\nu n_j)$ respectively to get [8, 36]

$$\frac{\partial}{\partial t} K_i^{\ j} = \beta^k K^j_{\ i,k} + K_k^{\ j}\beta^k{}_{,i} - K_i^{\ k}\beta^j{}_{,k} - \alpha_{|i}^{\ j} + \alpha[KK_i^{\ j} + R_i^{\ j} + g^{kj}T_{ik}], \tag{6}$$

$$R - K_j^i K_i^j + K^2 = 2\alpha^{-2}[T_{tt} - 2T_{ti}\beta^i + T_{ij}\beta^i\beta^j], \tag{7}$$

$$(K_j^i - \delta_j^{\ i}K)_{|i} = -\alpha^{-1}(T_{tj} - T_{jk}\beta^k), \tag{8}$$

where n^μ is the normal to the three-dimensional, constant t, hypersurfaces, $K = K_i^i$, R_j^i is the three-dimensional Ricci tensor and $|$ denotes covariant differentiation with respect to the three metric. These equations can be divided into evolution equations [(5) and (6)] and constraint equations [(7), and (8)]. The former determine the time changes of the geometric variables, while the letter impose constraints on them within a given hypersurface.

There are 16 geometric variables (g_{ij}, K_{ij}, β_i, α) and 16 geometric equations [eqs. (5)–(8)]. However, the coordinate freedom in general relativity allow us to freely specify four of these variables. This is naturally done in the ADM formalism by specifying α and β^i. The resulting 12 variables have to satisfy 16 equations. Although the system seems to be overdetermined, four of the equations are satisfied, in the continuum case, by virtue of the Bianchi identities. However, this relation breaks down in a finite-difference scheme [37, 40]. In such a case the equations are written on a spatial and temporal lattice and due to the noncommutative nature of finite-difference derivatives all the equations cannot be satisfied simultaneously in a trivial way (for example, to the same order in dx and dt). This leads to a serious ambiguity in finite-difference general relativity.

Before discussing the arbitrary choice between constraint and evolution equations I shall recount the geometric variables. In general there are $8 + 2N_{\text{mode}}$ geometric variables. N_{mode} is the number of modes of gravitational waves possible in the configuration which is studied. (There are no possible modes in a spherically symmetric configuration; one in a configuration with a plane reflection symmetry and two in the general case.)

Independent of the symmetry of the system one can use the coordinate freedom to reduce the number of free gravitational variables [5, 8, 13]. The basic physical motivation is to reduce the number of evolution equations to fit the degrees of freedom of the system, while the numerical motivation is to simplify the structure of the equations involved. Such a procedure eliminates a number, N_{coor} (up to four), of geometric variables by introducing elliptical equations (coordinate conditions) for α and β^i. (From a simple numerical point of view this approach has advantages since such an elimination can lead to great simplification of $R_j{}^i$ and to a simpler set of equations.) This can be done by imposing $f(g_{ij}) = \text{const}$ on the initial values and choosing α and β^i so that $\partial f/\partial t = 0$ later [22]. For example $g_{kj} = 0$ (for a particular kj) and $\partial g_{kj}/\partial t = 0$ [5].

It is possible to evaluate the constraint equations for covariant (in the three-dimensional sense) quantities like $\phi = (\det g_{ij})^{1/3}$ and W, the vector part of the extrinsic curvature tensor [9–12]. Equation (5) separates into an equation for ϕ and an independent simplified set of evolution equations for the "bare" metric $\tilde{g}_{ij} = \phi^{-1} g_{ij}$. However such a separation does not occur for the "bare" (i.e., transverse traceless) part of $K_j{}^i$. The latter fact makes such a scheme less attractive for practical numerical purposes.

An alternative approach is to solve the constraint equations for some of the variables in a noncovariant manner [5]. This leads to the following relations between the equations solved:

$$N_{\text{evol}} \geqslant 8 + 2N_{\text{mode}} - N_{\text{coor}} - N_{\text{cons}}\,, \tag{9}$$

where N_{evol} and N_{cons} are the number of evolution and constraint equations solved.

Different numerical schemes can be classified as follows:

free evolution [4, 33, 39]:	$N_{\text{cons}} = 0$
(Partially) constrained evolution:	$(1 \leqslant N_{\text{cons}} \leqslant 3)$ $N_{\text{cons}} = 4$
fully constrained evolution [5, 39]:	$N_{\text{evol}} = 2N_{\text{mode}}$
chopped evolution [37]:	Free or partially constrained evolution which is fully constrained every fixed time interval
covariantly constrained evolution:	Eq. (9) is satisfied as an inequality; the constraints are solved for covariant quantities.

A fully constrained evolution scheme has the nice physical property of correspondence between the number of hyperbolic equations and the number of physical degrees of freedom. It should be stressed that the coordinate conditions on α and β^i are an essential part of a fully constrained scheme. One has to use the full coordinate freedom to eliminate $N_{\text{coor}} = 4$ geometric functions. The specific choice of a coordinate system is not determined uniquely. It also cannot be defined in a covariant way. A covariantly constrained evolution, which uses York's procedure [10–12] or equivalent

methods, can be looked at as a limiting case of a chopped evolution for which the constraints are employed in a specific way.

The hydrodynamic equations are given by Eq. (2). For a perfect fluid, T_ν^μ has the form:

$$T_\nu^\mu = (p + \rho)\, u^\mu u_\nu + \delta_\mu^{\ \nu} p, \tag{10}$$

where u^ν is the four velocity. When projected along $u_\mu u^\nu$, $u_\mu(\delta_i^{\ \nu} - u^\nu u_i)$, and $(\delta_i^{\ \nu} - u^\nu u_i)$ $(\delta_\mu^{\ j} - u_\mu u^j)$, respectively [6, 14], Eq. (2) becomes analogous to the Newtonian hydrodynamic baryon number, energy, and momentum conservation equations:

$$\frac{\partial N}{\partial t} + \frac{\partial}{\partial x^i}(NV^i) = 0, \tag{11}$$

$$\frac{\partial E}{\partial t} + \frac{\partial}{\partial x^i}(EV^i) + p\frac{\partial}{\partial x^i}((-{}^{(4)}g)^{1/2}\, u^t V^i) + p\frac{\partial}{\partial t}((-{}^{(4)}g)^{1/2}\, u^t) = 0, \tag{12}$$

$$\frac{\partial S_i}{\partial t} + \frac{\partial}{\partial x^j}(S_i V^j) + (-{}^{(4)}g)^{1/2}\frac{\partial p}{\partial x^i} + \frac{1}{2}\frac{\partial {}^{(4)}g^{\mu\nu}}{\partial x^i}\frac{S_\mu S_\nu}{S^t} = 0. \tag{13}$$

$s_i = (\rho + p)\, u_i$ is the momentum density, $V^i = u^i/u^t$ is a three-dimensional velocity, and N, E, and S_i represent n, e, and s_i multiplied by $(-{}^{(4)}g)^{1/2}\, u^t$. (Projection of Eq. (2) along n^μ and into the three-dimensional, constant t, hypersurfaces yields a different set of hydrodynamic equations which have no simple physical interpretation.)

The matter terms in the geometry equations [Eqs. (6)–(8)] become

$$g^{kj}T_{ik} = -S_i(V^j + \beta^j) + \tfrac{1}{2}(p - \rho)\,\delta_i^{\ j}, \tag{14}$$

$$\alpha^{-2}(T_{tt} - 2T_{ti}\beta^i + T_{ij}\beta^i\beta^i) = (p + \rho)(\alpha u^t)^2 - p, \tag{15}$$

$$-\alpha^{-1}(T_{tj} - T_{jk}\beta^k) = \alpha S_j\,. \tag{16}$$

Cylindrical Symmetry

I use cylindrical coordinates (t, r, z, φ) with $-\infty < t < \infty, 0 < r < \infty, -\infty < z < \infty$, and $0 \leqslant \varphi < 2\pi$. There is no dependence on z and φ. The matter may rotate around the symmetry axis but we do not admit nontrivial z motion ($V^z = V^z(r, t)$). This excludes generation of Jordan–Ehlers–Kompaneetz [15, 16] waves and enables us to set $g_{rz} = g_{z\varphi} = 0$ and $\beta^z = 0$. When the matter is not rotating (or in the vacuum case) we can set $g_{r\varphi} = 0$ as well. In a rotating configuration $K_\varphi^{\ r} \neq 0$ and in general we cannot set $g_{r\varphi} = 0$. However, by a suitable coordinate transformation we can set $g_{r\varphi} = 0$ on the initial slice. We choose now $\omega \equiv \beta^\varphi$ to satisfy

$$\omega' = 2\alpha K_r^{\ \varphi} \tag{17}$$

with arbitrary boundry conditions (for convenience we can set $\omega(0, t) = 0$). Substitution of Eq. (17) in Eq. (5) gives $g_{r\varphi} = 0$ and the three metric remains diagonal

$$ds^2 = -\alpha^2 dt^2 + a^2(dr + \beta\, dt)^2 + \ell^2 dz^2 + e^2 r^2(d\varphi + \omega\, dt)^2. \tag{18}$$

The geometric equations (5)–(8) become

$$\dot{a} = -\alpha a K_r{}^r + (\beta a)', \tag{19}$$

$$\dot{b} = -\alpha b(K - K_r{}^r - K_\varphi{}^\varphi) + \beta b', \tag{20}$$

$$\dot{c} = -\alpha c K_\varphi{}^\varphi + \beta\left(c' + \frac{c}{r}\right), \tag{21}$$

$$\dot{K}_r{}^r = \beta K_r{}^{r\prime} + \omega' K_\varphi{}^r - \frac{1}{a}\left(\frac{\alpha'}{a}\right)' + \alpha\left[K K_r{}^r - \frac{1}{ab}\left(\frac{b'}{a}\right)' - \frac{1}{acr}\left(\frac{(cr)'}{a}\right)' - S_r(V^r + \beta) - \frac{1}{2}(\rho - p)\right]. \tag{22}$$

$$\dot{K}_z{}^z = \beta K_z{}^{z\prime} - \frac{1}{abcr}\left(\alpha\frac{cr}{a}b'\right)' + \alpha\left[K_z{}^z - \frac{1}{2}(\rho - p)\right], \tag{23}$$

$$\dot{K}_\varphi{}^\varphi = \beta K_\varphi{}^{\varphi\prime} - \omega' K_\varphi{}^r - \frac{1}{abcr}\left(\alpha\frac{b}{a}(cr)'\right)' + \alpha\left[K K_\varphi{}^\varphi - S_\varphi(V^\varphi + \omega) - \frac{1}{2}(\rho - p)\right], \tag{24}$$

$$\dot{K}_\varphi{}^r = \alpha[K K_\varphi{}^r - S_\varphi(V^r + \beta)], \tag{25}$$

$$\frac{1}{ab}\left(\frac{b'}{a}\right)' + \frac{1}{abcr}\left(\frac{b(cr)'}{a}\right)' + K_r{}^{r2} + K_\varphi{}^{\varphi 2} + K_r{}^r K_\varphi{}^\varphi + K_r{}^\varphi K_\varphi{}^r = -[(p + \rho)(\alpha u^t)^2 - p], \tag{26}$$

$$\frac{1}{b^2 cr}(b^2 cr K_r{}^r)' - \frac{b}{cr}\left(\frac{cr}{b}\right)' K_\varphi{}^\varphi - \frac{1}{b}(bK)' = \alpha S_r, \tag{27}$$

$$\frac{1}{abcr}(abcr\, K_\varphi{}^r)' = \alpha S_\varphi. \tag{28}$$

We use $\beta \equiv \beta^r$, $\dot{(\ )}$ denotes $\partial/\partial t$ and $(\ )'$ denotes $\partial/\partial r$.

The hydrodynamic equations become

$$\dot{N} + (NV^r)' = 0, \tag{29}$$

$$\dot{E} + (EV^r)' + p((-{}^{(4)}g)^{1/2} u^t) + p((-{}^{(4)}g)^{1/2} u^t V^r)' = 0, \tag{30}$$

$$\dot{S}_r + (S_r V^r)' + (-{}^{(4)}g)^{1/2} p' - \left\{\frac{\alpha'}{\alpha} S_t + \frac{a'}{a^3}\frac{S_r S_r}{S^t} + \frac{(cr)'}{(cr)^3}\frac{S_\varphi S_\varphi}{S^t} + \left(\beta' - \beta\frac{\alpha'}{\alpha}\right)\left(1 - 2\omega\frac{S_\varphi}{S^t}\right) S_r + \left(\omega' - \omega\frac{\alpha'}{\alpha}\right)\left(1 - 2\beta\frac{S_r}{S^t}\right) S_\varphi\right\} = 0, \tag{31}$$

$$\dot{S}_\varphi + (S_\varphi V^r)' = 0. \tag{32}$$

Coordinate Conditions[1]

The coordinate conditions are specified by α and β^i. This has already been partially done in Eq. (17) in which $\omega = \beta^\varphi$ was specified so that the metric remained diagonal. (This condition is important only for rotating matter configurations. In all other configurations $K_r{}^\varphi$ vanishes and Eq. (17) is satisfied trivially.)

α determines the foliation of space-time. The choice $K = 0$ (on all spatial slices) is called maximal slicing [9, 17]. This condition can be satisfied if $K = 0$ on the initial slice and $\dot{K} = 0$ later. Using Eq. (6),

$$\frac{\partial K}{\partial t} = \beta^k K_{,k} - \alpha^{i}_{|i} + \alpha[K^2 + R + \tfrac{5}{2}p - \tfrac{1}{2}\rho - (p + \rho)(\alpha u^t)^2]; \tag{33}$$

in cylindrical coordinates:

$$\dot{K} = \beta K' - \frac{1}{abcr}\left(\frac{bcr}{a}\alpha'\right)' - \alpha\left[\frac{2}{ab}\left(\frac{b'}{a}\right)' + \frac{2}{acr}\left(\frac{(cr)'}{a}\right)' + \frac{2b'(cr)'}{a^2bcr} - K^2 + \tfrac{1}{2}\rho - \tfrac{5}{2}p + (p + \rho)(\alpha u^t)^2\right]. \tag{34}$$

Equation (34) is used as an elliptical equation for α. The maximal slicing condition is useful in collapse calculations since it slows the evolution in regions that approaches a singularity [18, 19, 22]. In addition, it eliminates one geometrical variable.

In most cosmological problems it is impossible to choose maximal slicing [38]. (In a Friedmann Universe there is only one maximal slice—the three-dimensional hypersurface at maximal expansion.) Another convenient choice is a constant K (constant mean curvature) slicing. Again Eq. (34) becomes an elliptical equation for α with $\dot{K} = \text{const}$ [43]. (Note that it is not yet concluded whether such slices exist in the general case [20, 21]).

A covariant choice of β^i was suggested by Smarr and York [22]. Their coordinate condition is

$$\left[\frac{\partial}{\partial t} g^{1/3} g^{ij}\right]_{|j} = 0 \tag{35}$$

which leads to a second-order elliptic equation for β^i. When combined with the maximal slicing condition [Eq. (34)] and for nonrotating systems ($\omega = 0$) this gives rise to

$$\frac{2}{3}\left[\frac{1}{abcr}(abcr\beta')\right]' - \beta\left[\frac{a}{b}\left(\frac{b'}{a}\right)' + \frac{a}{cr}\left(\frac{(cr)'}{cr}\right)'\right] + \alpha' K_r{}^r - \alpha S_r = 0. \tag{36}$$

This coordinate condition attempts to minimize the coordinate shear and it follows the spirit of York's [10–12] covariant treatment of the constraint equations. However, it does not lead to any simple algebraic elimination of geometric variables.

[1] These are also called gauge conditions [13].

Out of the many possible "simplifying" coordinate conditions I have used, isothermal coordinates [5][2] $a = b$ which lead to

$$\beta' = \alpha(2K_r{}^r + K_\varphi{}^\varphi - K) \tag{37}$$

and the canonical coordinate condition $bc = 1$

$$\beta = \alpha r(K - K_r{}^r). \tag{38}$$

The importance of the second condition is in its potential simple extension to general cylindrical cases (i.e., with two modes of polarization) and to two-dimensional axisymmetric rotating configurations. Note that in this case $a = (\det g_{ij})^{1/2}/r = \phi^{3/2}/r$; however, solving the Hamiltonian constraint for a is not equivalent to evolution of the bare metric g_{ij} and calculation of ϕ from the Hamiltonian constraint. Other possible choices, along the same idea, are $bc = a$, $c = 1$, etc.

The trivial coordinate condition $\beta^i = 0$ was studied as well. When combined with maximal slicing it yields

$$\frac{\partial}{\partial t}\,{}^{(3)}g = \frac{\partial}{\partial t}(a^2\ell^2c^2) = 0 \tag{39}$$

and it could be considered therefore as a "simplifying" gauge. However, this relation was not used to eliminate a metric function in the numerical procedure.

III. Numerical Methods

Our finite-difference scheme is second-order accurate in space and first-order accurate in time. (We use a staggered temporal grid structure, so that in principle our scheme can be considered as second order accurate in time as well. However, there was no attempt to retain this accuracy systematically. The spatial grid is staggered and is described in Fig. 1 [3, 6]. The temporal staggering is described in Fig. 2. Loosely extrinsic curvature components and the shift vector are calculated at $t + \frac{1}{2}dt$ points relative to the metric components and the lapse function which are calculated at integer dt intervals, and in the same way momenta and velocities are calculated at $t + \frac{1}{2}dt$ points relative to the density, pressure, and specific energy.

In the following discussion the numerical grid points will be denoted by capital letters, while the coordinates are denoted by lowercase letters.

Finite-Difference Scheme for the Evolution Equations

A general form for both hydrodynamic and geometric evolution equations is

$$\dot{y} = (Vy)' + xy + \text{source (no linear terms in } y). \tag{40}$$

[2] Isothermal coordinates which were first introduced to numerical relativity by Wilson [5] are sometimes denoted [13, 39] as Wilson gauge.

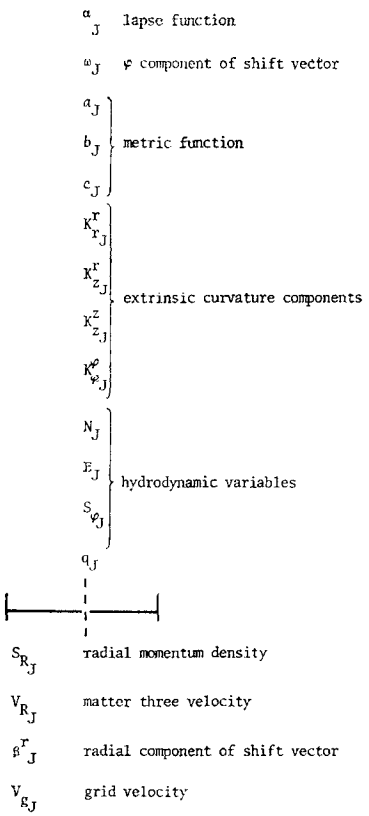

FIG. 1. The spatial staggering of the various variables. Note that only the variables S_r, V_r, β^r, and V_g are defined on the axis ($r = 0$).

V stands for $-(V^r - V_g)$, V_g is the grid velocity (note the minus sign) in the hydrodynamic equations and for $(\beta + V_g)$ in the geometric ones. The source term may include terms like y^2 but all the linear terms in y are included in xy. (Equations (13–(17) are cast into this form by addition and subtraction of $y(\beta + V_g)'$.)

The finite-differencing scheme follows Wilson's approach (compare to [5, 6] for details of the numerical method) which is motivated by methods developed for Newtonian hydrodynamics. The first term (the flux term) is evaluated so that y is a conserved quantity. A weighted average of first- ("donor" type) and second-order terms is used. The weighting factor is such that the flux is second order accurate when the gradient of y is small and it is of "donor" type when the gradient is large. This is done to handle hydrodynamic shocks but it proves to work equally well for geometric quantities.

$$\text{flux}_{I+1/2} = dt\, V_{I+1/2}[(1 - w)\, \bar{y}_{I+1/2} + w y_D], \tag{41a}$$

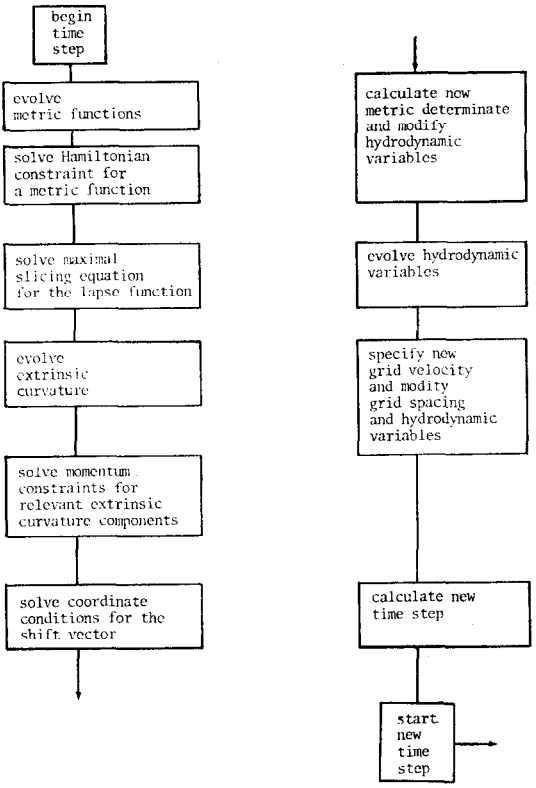

FIG. 2. The flow chart of the main evolution loop. The temporal staggering of the variable is defined implicitly by this chart.

where

$$w = \begin{cases} |(y_{I+1} - y_I)/(|\, y_{I+1}\,| + |\, y_I\,|)| & \text{for } |(y_{I+1} - y_I)/(|\, y_{I+1}\,| + |\, y_I\,|)| < W_{\max} \simeq \frac{1}{2} \\ 1 & \text{for } |(y_{I+1} - y_I)/(|\, y_{I+1}\,| + |\, y_I\,|)| > W_{\max} \simeq \frac{1}{2}, \end{cases} \tag{41b}$$

$$\bar{y}_{I+1/2} = (\tfrac{1}{2} + V_{I+1/2} dt/\Delta r)\, y_I + (\tfrac{1}{2} - V_{I+1/2}\, dt/\Delta r)\, y_{I+1}\,, \tag{41c}$$

and

$$y_D = \begin{cases} y_{I+1}\,, & V_{I+1/2} > 0 \\ y_I\,, & V_{I+1/2} < 0. \end{cases}$$

The overall finite-difference form of Eq. (40) is

$$y_I^{N+1} = \frac{(\text{flux}_{I+1/2} - \text{flux}_{I-1/2})/\Delta r_I + (1 + \frac{1}{2} dt X_I)\, y_I{}^N + dt\ \text{source}_I}{(1 - \frac{1}{2} dt X_I)} \tag{42}$$

Hydrodynamics

The hydrodynamic equations, Eqs. (29)–(32), are supplemented by the equation of state. For simplicity we use

$$p = (\Gamma - 1)\, e. \tag{43}$$

In order to handle hydrodynamic shocks we add an artificial viscosity q to the pressure (see, for example, Richtmyer and Morton [23] and Wilson [14]). It is treated as part of the pressure and it is added to p in the geometric as well as in the hydrodynamic, equations. q is defined as

$$q_l = \begin{cases} l^2 n_l u^l{}_l (V_{l+1/2} - V_{l-1/2})^2, & V_{l+1/2} - V_{l-1/2} > 0,\ (n_l - n_{l-1})\, V_{l-1/2} < 0, \\ & \text{and } (n_{l+1} - n_l)\, V_{l-1/2} < 0; \\ 0 & \text{otherwise.} \end{cases} \tag{44}$$

l is a constant of order unity ($l \simeq 1$–2).

The second and third conditions which are added to the usual shock condition [23, 14],

$$V_{l+1/2} - V_{l-1/2} > 0, \tag{45}$$

are needed in gravitationally collapsing configurations.

Equation (29) is solved for N. It is later rescaled by $\tilde{r}_l d\tilde{r}_l / r_l dr_l$; $\tilde{r}_l = r_l + V_{gl} dt$, in order to take care of corrections due to the grid motion. Similarly Eqs. (31) and (32) are solved for S_r and S'_φ. Following Wilson [14], the special form of p is used to combine the p (but not the q) part of the third and fourth terms in Eq. (30) with the first and second ones and to solve the equation for $[(-{}^{(4)}g)^{1/2} u^t]\, E^{\Gamma-1}$; this is rescaled later with the needed powers of $-{}^{(4)}g$ and u^t and by $\tilde{r}_l d\tilde{r}_l / r_l dr$.

Geometry

The various choices for evaluation of the geometric variables are:

a—solved from Eq. (19) (evolution) or from Eq. (26) (Hamiltonian constraint).

b—Eq. (20) (evolution)—only when relevant, i.e., for $b \neq a$, $b \neq 1/c$, etc.

c—Eq. (21) (evolution) or (26) (Hamiltonian constraint).

$K_r{}^r$—Eq. (22) (evolution) or (27) (momentum constraint).

$K_z{}^z$—Evaluated as $K - K_r{}^r - K_\varphi{}^\varphi$.

$K_\varphi{}^\varphi$—Eq. (24) (evolution)

$K_\varphi{}^r$—Eq. (25) (evolution) or (28) (momentum constriant).

α and β^i are solved using Eqs. (34)–(38), depending on the particular coordinate choice.

Grid Velocity

In calculations involving matter motion it is necessary that in particular, in gravitational collapse calculations, the numerical grid will follow, to some extent, the matter

motion. Otherwise, the matter will be concentrated in one grid cell and the computation could not proceed. This can be done by a Lagrangian[3] coordinate choice $\beta^r = V^r$ [24]. However, in order to maintain the coordinate freedom for the geometry Wilson introduces a grid velocity [5] which follows the matter motion and prevent this phenomenon. A grid point r_I moves during a time step dt from r_I to $r_I + V_{gI}dt$, where V_{gI} is a freely specified function. A term $V_g F'$ is added to the right-hand side of the evolution equations ($\dot{F} =$) to describe the change $F_I = F(r_I) \to F(r_I + V_{gI}dt)$. (In the hydrodynamic equations we subtract V_g from V^r and later rescale N, E, and S_i in order to take care of the unnecessary addition of the terms: NV_g', etc. which are introduced in this way,)

It should be emphasized that the grid velocity is not equivalent to the shift vector. The grid velocity transforms the observer's (grid points) relative to the coordinates from one time slice to another, while the shift vector transforms the coordinates as well as the local observation tetrad.

The grid velocity can be freely specified. The choice $V_{gI}^j = V_I^j$ yields a numerical Lagrangian scheme. (The coordinates are not Lagrangian but the grid points are comoving with the matter and the flux terms in the hydrodynamic equations disappear.) Both Lagrangian methods ($\beta^j = V^j$ and $V_g{}^j = V^j$) are not adequate to follow the propagation of the generated gravitational waves. The coordinates (or the grid points) that follow the matter, collapse with it, and there is no "room", i.e., no exterior vacuum region in which the wave can "freely propagate." This problem does not occur in spherical Lagrangian schemes [2, 25, 26] in which there is no gravitational radiation. An Eulerian [3] grid is needed, at least at the outer edges of the numerical grid, in order to observe the propagation of gravitational waves.

A solution for both problems is achieved by specifying the grid velocity in such a way that it follows the matter velocity for a few inner grid points while vanishing on the outer boundary. In the intermediate region the grid velocity is varied smoothly for example by demanding that $\Delta r_{I+1} = \text{const}\, \Delta r_I$.

A Lagrangian–Eulerian scheme whose numerical Lagrangian inner part follows the matter while sliding on a numerically Eulerian outer grid may be the ultimate solution for both problems. Such a scheme is now being studied.

Boundary Conditions

A spacelike slice is usually infinite (or at least very large in the case of a closed Universe). Our grid is finite and usually limited to 100 (or less) points. One must, therefore, provide boundary conditions—or a specific scheme for solution of the equations on the inner (axis) and outer boundaries of the numerical grid. (An alternative approach, suggested by Penrose [27], is to use compactified space–time.) While

[3] A Lagrangian observer is comoving with the matter. The extension of the definition of an Eulerian observer from Newtonian to relativistic hydrodynamics is somewhat ambiguous. In contrast to [3, 42] I define an Eulerian observer as any non-Lagrangian observer which is at rest with respect to the coordinate system in use. Such an observer is called a coordinate observer by [42].

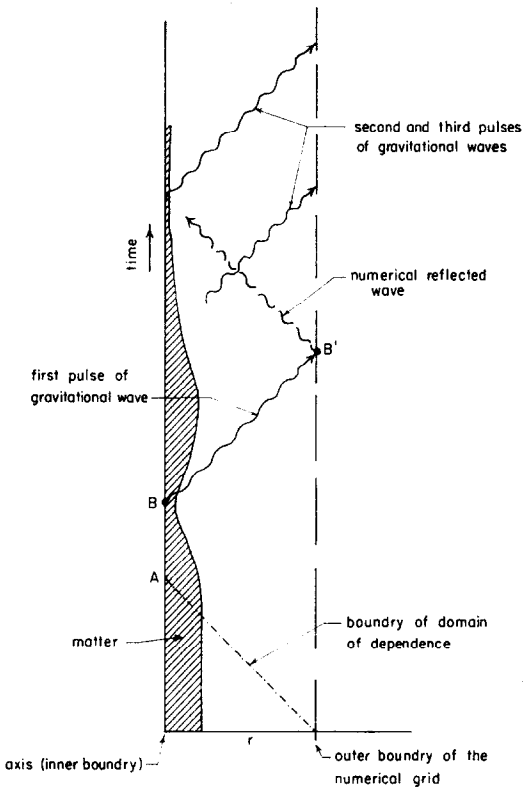

FIG. 3. The exact and the numerical domains of dependence. The exact domain of dependence ends at point A, which is usually too short for any significant variation in the configuration. When there is no incoming radiation, a simple boundary condition suffices to continue the calculations to point B′ at which reflection from the numerical boundary of radiation generated at B begins. With a proper outgoing boundary condition the solution can be continued beyond B′.

the inner boundary conditions can be determined from analytic considerations, there are no such rules for the outer boundary conditions.

In principle, when data is given on a finite initial slice the Einstein equations can be integrated only within the domain of dependence [22, 28] of this region (see Fig. 3). However, when the exterior is empty and does not contain ingoing gravitational waves, one can expect to be able to continue the calculation beyond this domain of dependence. It may be continued until the perturbations (such as gravitational waves) reach the outer boundary of the grid (employing smooth boundary conditions which do not generate gravitational waves). Reflection may destroy the numerical continuation of the solution beyond this point. It is very useful to be able to continue the calculation further. Boundary conditions which enable the waves to propagate out of the grid without reflection are essential for this. The following outgoing wave boundary conditions for a function f is used:

$$f_{I+1}^{N+1} = f(r_{I+1}, t + dt) = \frac{r_{I+1} - \Delta}{r_{I+1}} f(r_{I+1} - \Delta, t)$$

$$= \frac{r_{I+1} - \Delta}{r_{I+1}} \left[f_{I+1}^{N} \left(1 - \frac{\Delta}{\Delta r}\right] + f_I^N \frac{\Delta}{\Delta r} \right), \tag{46a}$$

$$\Delta = dt(\alpha/a - \beta) \tag{46b}$$

($\Delta = dt(\alpha/a - \beta - V_g)$ when V_g does not vanish on the edge of the grid) where $\Delta r_I = r_{I+1} - r_I$. Equation (46) corresponds to propagation of a cylindrical outgoing wave along a null geodesic. This condition is used for the extrinsic curvature K_j^i components. Equation (46a) must be modified when the unperturbed value of the function t does not vanish at the boundary. For example, a similar expression but without the damping factor $(r_{I+1} - \Delta)/r_{I+1}$ is used for the metric component functions a, b, and c for vacuum cases. (For these quantities it is best to use this condition for the two outermost points.) When there is matter, the "static" exterior background metric is not asymptotically flat. Usually the contribution of this "static" curvature is dominant (compared to the effect of the gravitational waves). Correspondingly, we use quadratic interpolation for the metric functions a, b, and c in this case.

In some cases this interpolation causes instability on the outer boundary. This behavior should not happen in asymptically flat space–times.

The outer boundary condition for $\alpha(\alpha = 1)$ is arbitrary and it amounts to scaling of the t coordinate (the situation is different in an asymptotically flat space–time where one chooses $\alpha = 1$ so that t will be the observer time at infinity). The inner boundary conditions (on the axis) are $a(0, t) = c(0, t)$ and $K_r{}^r(0, t) = K_\varphi{}^\varphi(0, t)$ (these are necessary for local flatness) and $a'(0, t) = b'(0, t) = c'(0, t) = \alpha'(0, t) = \beta(0, t) = \omega(0, t) = 0$ (which are necessary to avoid divergences on the axis).

Time Step

The time step, dt, is determined by the propagation of gravitational waves [6], i.e., it is chosen so that a null geodesic will not advance more than a fraction f_g (usually a third) of a grid spacing Δr during a single step:

$$dt_g = f_g \Delta r \Big/ \left(| \beta^r | + \frac{1}{a} \left(\alpha^2 - \sum{}' \beta_j \beta^j \right)^{1/2} \right), \tag{47}$$

where the sum $\sum'$ is only over cyclic coordinates, i.e., only over φ ($\beta^z = 0$). In order to take account of the grid motion β^r is replaced by $(\beta^r + V_g)$. One may note the similarity between this formula and the standard relation for a hydrodynamic time step:

$$dt_h = f_h \Delta r / (| V^r | + C_s). \tag{48}$$

The analogy between the shift vector (coordinate motion) and the fluid flux (matter motion) and between the "speed of light," $(\alpha^2 - \sum' \beta_j \beta^j)^{1/2}$, and the fluid speed of sound, C_s, is clear. As the gravitational time step is much shorter than the hydrodynamic one the resulting hydrodynamic flow is very smooth. One can use the hydrodynamic time step in situations in which the gravitational variables are changing very slowly.

Additional limitation on the hydrodynamic time step are discussed by Wilson [6].

Initial Values

The initial values are not completely arbitrary. The constraint equations [Eqs. (7) and (8) or (26)–(28)] must be satisfied on every time slice and in particular on the initial one. O'Murdacha and York [10, 11] and York [12] suggested two covariant methods for solving the initial value problem for strong field cases.

Another possibility [5] used here is to specify the number, energy, and momentum densities and three metric and extrinsic curvature components. The other three (usually one metric and two extrinsic curvature components) are solved from the constraint equations (the z momentum constraint equation is satisfied identically in this configuration). The same procedure is done every time step in a fully constrained scheme. It is not "guaranteed" that there will always be a solution, and in particular that there will be a physically reasonable one. However, for an almost Newtonian initial configuration such a solution was always found. In cosmological problems these methods failed in some cases. The specification of only some of the initial variables can produce unanticipated aphysical values in the remaining variables when the constraint equations are solved. This difficulty is inherent to all methods.

IV. Vacuum Solution—Einstein–Rosen Waves

The general vacuum cylindrical solution of Einstein's equations are the Jordan–Ehlers–Kompaneet waves [15, 16] (see also Thorne [29] and Piran [30] for discussion). These waves have two modes of polarization. The general Jordan–Ehlers–Kompaneet waves cannot be described by a diagonal three metric. Both K_r^{φ} and K_z^{φ} do not vanish and cannot satisfy Eq. (17) and an analog equation with K_z^{φ} simultaneously. The same problem prevents the diagonalization of the metric in axially symmetric rotating configurations. The line element used here Eq. (18)) can describe only a special case of these waves. These are the Einstein–Rosen waves [31] which have one polarization mode. The Einstein–Rosen line element is

$$ds^2 = e^{2(\gamma-\psi)}(-dT^2 + dR^2) + e^{2\psi}dz^2 + R^2e^{-2\psi}d\varphi^2 \tag{49}$$

with

$$\frac{\partial^2\psi}{\partial T^2} = \frac{1}{R}\frac{\partial}{\partial R}\left(R\frac{\partial\psi}{\partial R}\right), \tag{50a}$$

$$\frac{\partial \gamma}{\partial R} = R\left[\left(\frac{\partial \psi}{\partial T}\right)^2 + \left(\frac{\partial \psi}{\partial R}\right)^2\right], \tag{50b}$$

$$\frac{\partial \gamma}{\partial T} = 2R\frac{\partial \psi}{\partial T}\frac{\partial \psi}{\partial R}. \tag{50c}$$

Equation (50a) is a cylindrical wave equation in flat space–time and an Einstein–Rosen wave packet can be written as

$$\psi(r, t) = \int d\tilde{\omega}\, A(\tilde{\omega})\, e^{i\tilde{\omega}t} J_0(\tilde{\omega} r). \tag{51}$$

With this analytic solution available a cylindrical vacuum system becomes an excellent arena for testing various numerical schemes.

Thorne [29] defined the cylindrical energy (C energy) by geometrical quantities. For a metric described by Eq. (18) this equals

$$C = \pi\left[1 - \left(\frac{(\ell c r)'}{a\ell}\right)^2 + \frac{(\ell c r K_r{}^r)^2}{a^2}\right]. \tag{52}$$

The C energy corresponds to the total energy per unit length within a cylinder of radius r. (Note that in this units $C \leqslant \pi$ and for $G = 1$, $C \leqslant \frac{1}{8}$.)

In the following discussion the C energy is used to study the propagation of gravitational waves pulses and the generation of gravitational waves by collapsing matter. As such C energy density is not a unique measure of the gravitational wave energy, for there is none [30, 31]. There was no attempt to use alternative methods [3, 13]. Conservation of the C energy is an essential feature of a good cylindrical numerical code.

A numerical solution of the propagation of an Einstein–Rosen wave packet is shown in Fig. 4. The initial data is time symmetric ($K_j{}^i = 0$), the coordinates are isothermal ($g_{rr} = g_{zz}$), and the perturbation in $a = g_{rr}{}^{1/2}$ has the form

$$a(r, 0) = 1 + A_0 r^2 \exp\left(-\left(\frac{r - r_0}{\Delta}\right)^2\right) \tag{53}$$

with Δ, r_0, and A_0 such that the perturbation extends over 10–15 grid points. The total C energy is $0.65 \simeq 0.20$ of the maximal possible C energy. (Calculation with $C = 1.81$ displayed the same behavior.) The other metric function, c, is calculated from Eq. (21). The initial C energy density profile has two humps, so what appears, in g_{rr}, as a single wave packet is actually composed of two packets. There are two outgoing and two ingoing waves. It is interesting that the behavior of the metric function, c (or any of the other metric or extrinsic curvature components), does not display all the details of the propagation of the wave packet. Those could be observed only in the C energy density or in $K_j{}^i K_i{}^j$.

The solution presented in Fig. 4 is calculated using a fully constrained scheme in which only two functions ($a = g_{rr}{}^{1/2} = g_{zz}{}^{1/2}$ and $K_\varphi{}^\varphi$) are evolved. The other func-

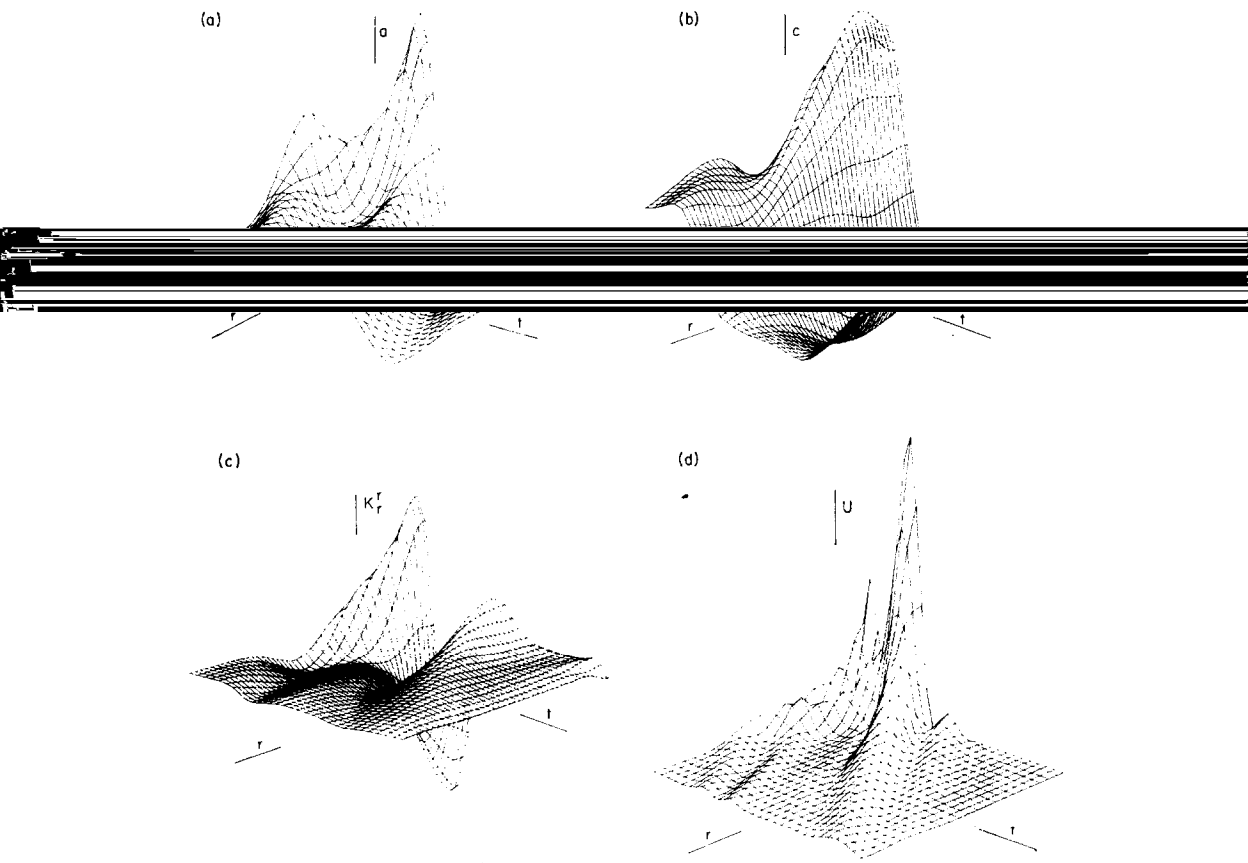

FIG. 4. A numerical solution for Einstein–Rosen waves using a fully constrained evolution and an isotropic coordinates. (a) The metric function $a = g_{rr}^{1/2} = g_{zz}^{1/2}$; (b) the metric function $c = g_{\varphi\varphi}^{1/2}/r$; (c) the extrinsic curvature component K_r^r; (d) the C energy density, U.

tions are either eliminated by the coordinate choice r ($a = b$ from Eq. (37) and $K = 0$ from Eq. (36)) or calculated from the constraint equations ($c = g_{\varphi\varphi}^{1/2}/r$ and K_r^r).

The results of this scheme are in excellent agreement with an analytic solution calculated using Eq. (51). (The difference is too small to be observed on the scale of Fig. 4.) The scheme is numerically stable. This stability depends on the temporal staggering. (See Fig. 2.) The outgoing wave boundary conditions enable the calculations to be continued until the wave packet propagate out of the grid.

Several variations of this scheme were tried. These include free as well as chopped evolution and include partially constrained schemes and different coordinate choices.

Evolution Versus Constraint Equations

The scheme contains more numerical noise when the constraint equations are replaced by evolution equations. However, the results are still close to the analytic

solution and to the numerical solution which is based on the constraint equations. The numerical noise on the boundary sometime leads to numerical instability in that region.

Evolution of $K_r{}^r$. There are no significant changes from a constrained solution. The difference in the metric functions between these solutions and the previous one cannot be observed on the scale of Fig. 4. The only observed difference is a non-vanishing $K_r{}^r$ near the axis, which in turn leads to nonvanishing stationary C energy density in that region. A measure of the accuracy is the deviation of $K_r{}^r(0, t)$ from $K_\varphi{}^\varphi(0, t)$ [39]. When the extrinsic curvature is large, this difference is 1–3 % of $K_r{}^r(0, t)$. (This ratio increases when $K_r{}^r(0, t)$ decreases at late times, but the magnitude of the difference remains the same throughout the rest of the calculations.) Another measure of the accuracy of this scheme is given by the deviation in the momentum constraint equation from zero. This deviation is shown in Fig. 5. There are three clear feature; the deviation does not grow after an initial period of fast increase (i.e., there is no instability). The deviation oscillates in space, and to some extent in time. The maximal value of this deviation is about 10 % of the maximal value of $K_r{}^{r\prime}$.

Chopped $K_r{}^r$ *evolution.* Results of chopped $K_r{}^r$ evolution are shown in Fig. 6. Deviations from zero in the momentum constraint equation are almost completely suppressed by calculation of the momentum constraint once every 100 time steps. This is accompanied by an improved behavior of $K_r{}^r$ near the axis and by vanishing of the C energy density near the axis at late times. It is important to note that the constraint calculations do not introduce any discontinuity in $K_r{}^r$ or in any other quantities (thus removing a serious objection to the chopped evolution scheme).

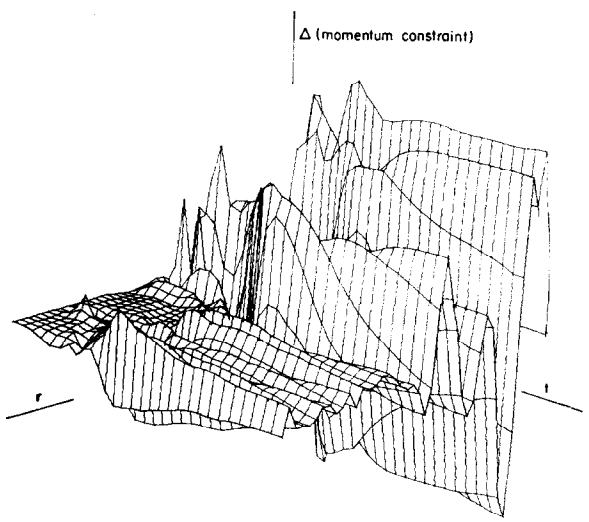

FIG. 5. The deviation from the r component of the momentum constraint equation in a partially constrained scheme when this constraint is not enforced.

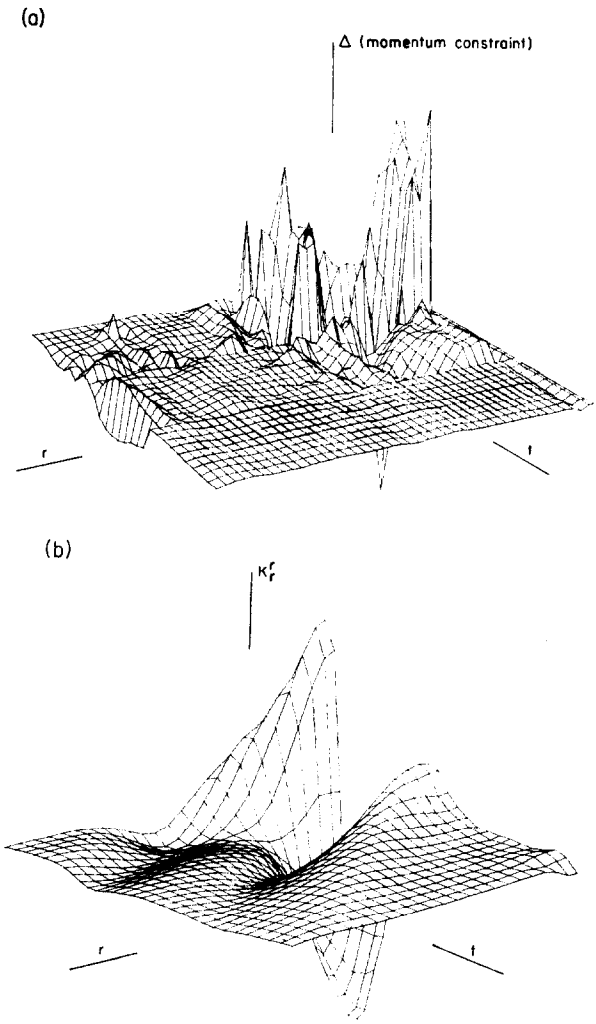

FIG. 6. Results of a $K_r{}^r$ chopped evolution scheme: (a) the deviations from the momentum constraint; (b) the extrinsic curvature component $K_r{}^r$.

Evolution of $c = g_{\varphi\varphi}{}^{1/2}/r$. The scheme contains more numerical noise when c is calculated from an evolution equation. While there are still no significant deviations in the evolution of the metric components the C energy density displays a small stationary C energy peak (See Fig. 7.) The deviation from the Hamiltonian constraint increases very rapidly near the axis at the beginning of the calculation (following the ingoing wave). At latter times, when this wave propagates outwards, it decreases slightly near the axis while at the exterior region it oscillates both in space and time. The relative deviation from the Hamiltonian constraint is much larger than that of the momentum constraint equation. Near the axis the deviation is of the same order of

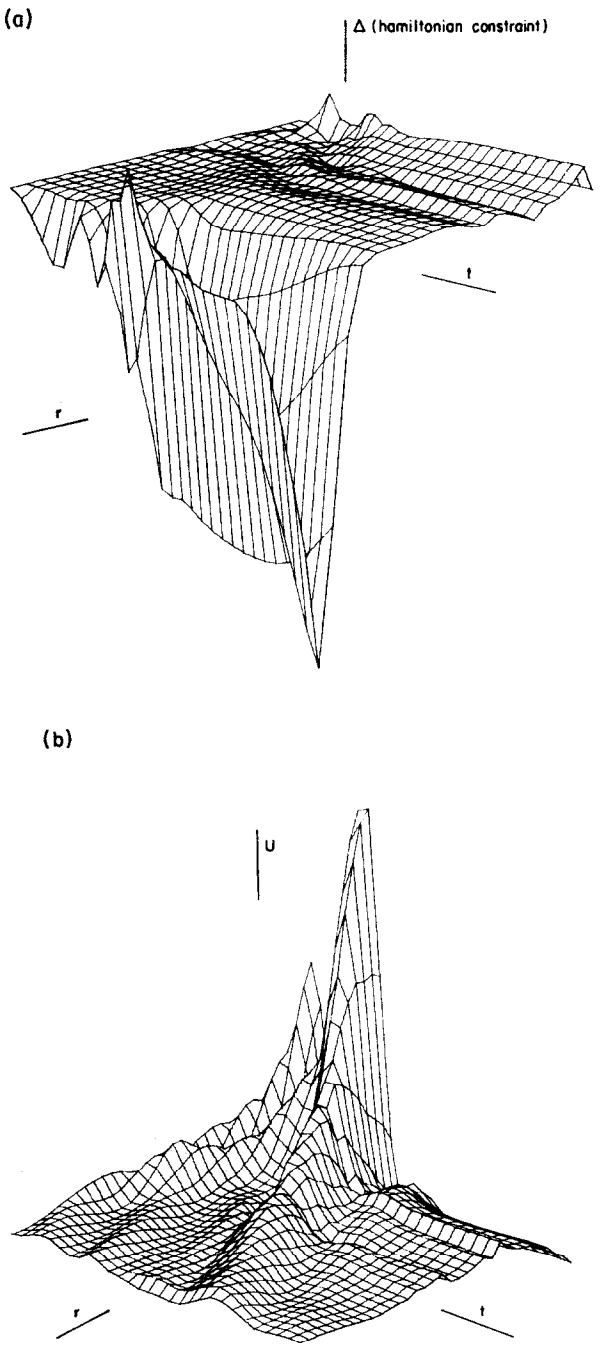

FIG. 7. A partially constrained scheme in which the Hamiltonian constraint is not enforced: (a) the deviation from the Hamiltonian constraint equation; (b) the C energy density.

magnitude as the $K_j^i K_i^j$ term. This is in part due to temporal staggering. In spite of the growth of the deviation from Hamiltonian constraint near the axis, the difference between a and c on the axis remains less than 10^{-3} throughout the calculation.

A simple outgoing wave boundary condition is not adequate for c. This phenomenon is a result of our coordinate choice and of the asymptotic behavior of cylindrical metric functions. It causes large ocsillations in c near the outer boundary. These are accompanied by a large deviation from the Hamiltonian constraint, which is not displayed in Fig. 7. However, mainly due to the outgoing nature of the boundary conditions these instability do not propagate inwards and the inner part of the solution remains remarkably good.

Chopped c Evolution. A chopped c evolution has the same features of a chopped K_r^r evolution. The constraint is imposed by calculations of c from the Hamiltonian constraint equation every 100 time steps. This is sufficient to suppress the growth of the deviation (see Fig. 8), and to wipe out the superfluous C energy density peaks. Again this is not accompanied by any discontinuity in c or in the other variables.

Free Evolution. Evolution of K_r^r and c; the boundary conditions presented here are not good enough for this combination. The instability that was observed on the boundary when only c was evolved causes now oscillations in K_r^r and a global instability. This behavior could not be suppressed by a chopped evolution. However, this is basically a boundary problem and the interior part of the solution is not affected by this instability. This boundary problem will, probably, disappear in an asymptotically flat configuaration. A reasonable solution can still be calculated as long as the

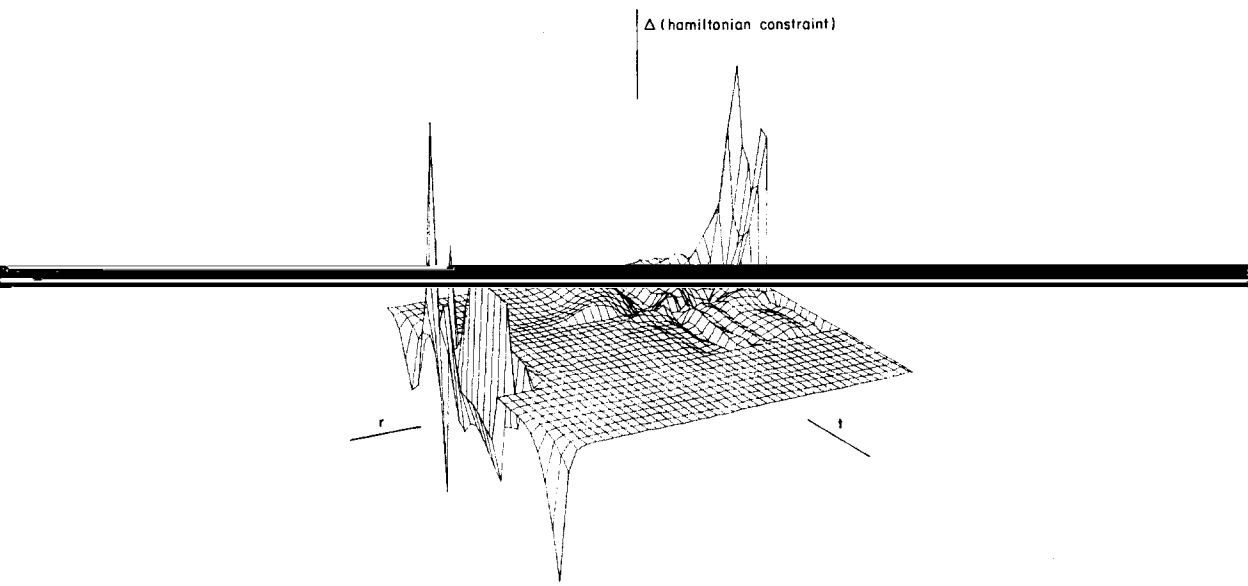

FIG. 8. The deviation from the Hamiltonian constraint in a chopped c evolution scheme.

outgoing wave does not reach the outer boundary. Centrella [32] who used a free-evolution scheme for plane symmetric periodic configuration did not encounter this problem.

Coordinate Choices

The different coordinate conditions change the structure of the geometric equations. For example when $\beta = 0$, the "geometric flux" terms disappear from the geometric equations, and when canonical coordinates are used, the second derivatives of the metric functions disappear from the Hamiltonian constraint equation.

Results of wave propagation with $\beta = 0$ are shown in Fig. 9. (On the initial slice $a = b$ and the initial perturbation is given by Eq. (53).) The deviation from an exact solution are, as with the previous schemes, too small to be observed on the scale of Fig. 9. The scheme is constrained, but not fully constrained—there are three evolution equations while only two are really essential. Since K and β vanish the determinant of the three metric, ${}^{(3)}g$, should be conserved. (In principle, this could be used in order to evaluate algebraically one of the metric functions and to construct a fully constrained scheme.) The value of ${}^{(3)}g$ is conserved within 1/4 % (compare to [41]).

The conservation of the metric ${}^{(3)}g$ makes it impossible (unless ${}^{(3)}g = 1$ on the initial slice) for the metric to become a flat cylindrical metric after the wave packets have propagated. The region near the axis becomes flat but it is described in curved coordinates. This example manifests the need to consider the expected form of the final solution and not just simply when the coordinate choice is made. See [39] for discussion of a similar behavior for Brill Waves.

A comparison of Figs. 9 and 4 shows that for $g_{rr} = g_{zz}$ the wavelike behavior appear in $g_{rr}(=g_{zz})$, while $g_{\varphi\varphi}$ describes the overall curvature. In this case the wavelike behavior appears in g_{zz}.

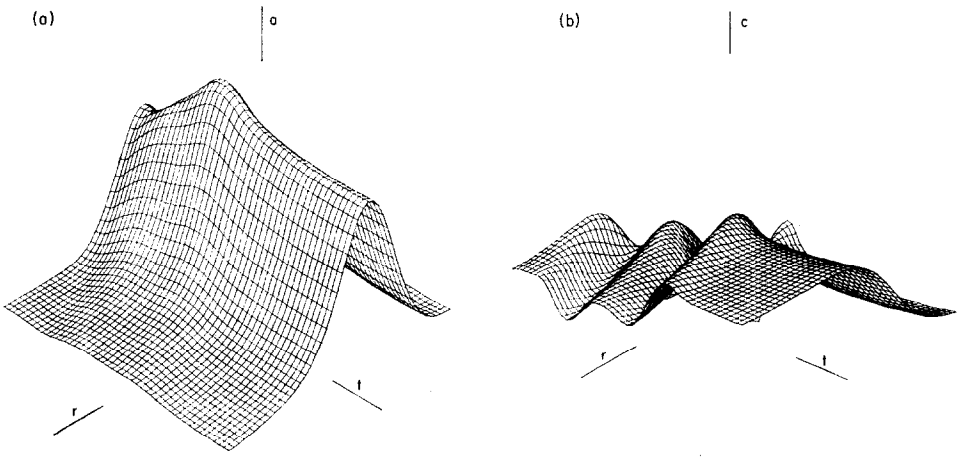

FIG. 9. A partially constrained scheme with $\beta = 0$: (a) the metric function $a = g_{rr}^{1/2}$; (b) the metric function $c = g_{zz}^{1/2}$.

Results of calculations using canonical coordinates ($bc = 1$) are shown in Fig. 10. This is again a fully constrained scheme; the Hamiltonian constraint is solved for a (using fourth-order Runge–Kutta integration) and c is calculated from an evolution equation. The initial perturbation is expressed as a perturbation in c:

$$c(r, 0) = 1 + C_0 r^2 \exp\left(-\frac{(r - r_0)^2}{\Delta}\right). \tag{54}$$

Like the ($a = b$) scheme, and unlike the $\beta = 0$ scheme the final metric is a flat, cylindrical metric. On the other hand, wavelike behavior appears now both in a and in c. Actually a and c have very similar behavior.

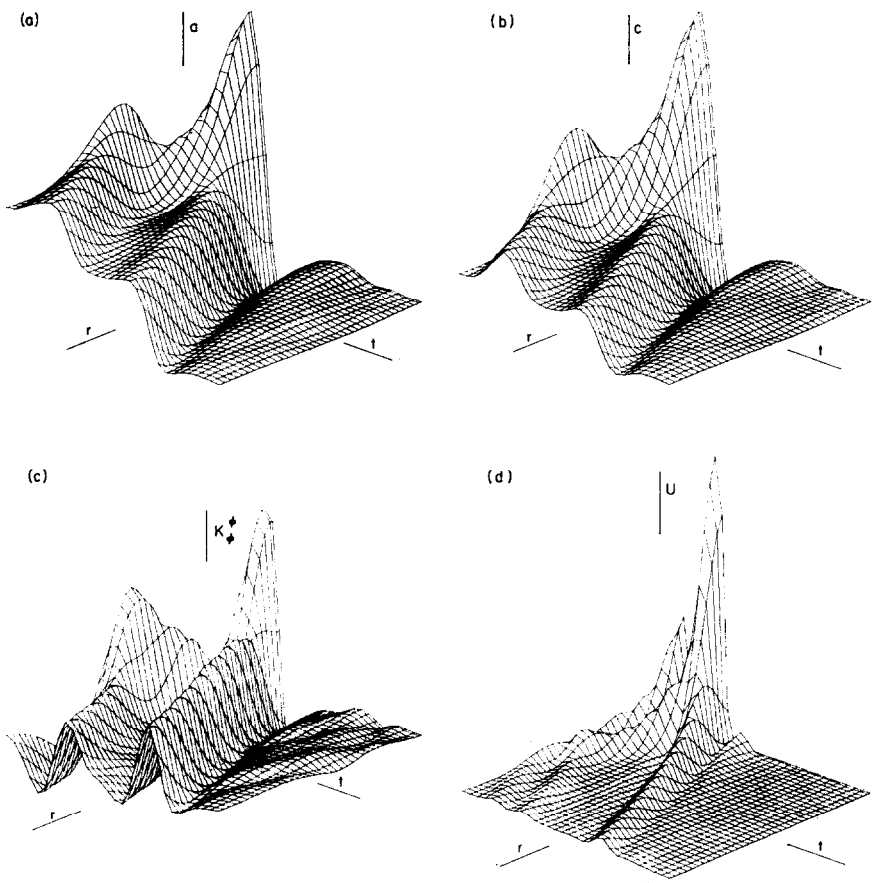

FIG. 10. A fully constrained scheme for Einstein–Rosen waves, using a canonical coordinate ($\ell c = 1$): (a) the metric function $a = g_{rr}^{1/2}$; (b) the metric function $c = g_{\varphi\varphi}^{1/2}/r$; (c) the extrinsic curvature component $K_\varphi{}^\varphi$, (d) the C energy density.

The minimal shear [Eq. (36)] solution was very similar to the $\beta = 0$ one. The shift vector remained very small and it had no noticeable effects on the behavior of any of the metric functions.

Geometric Artificial Viscosity

Unlike hydrodynamics, there is no physical motivation for introducing a geometric artificial viscosity. However, artificial geometric viscosity was found useful in some recent calculations [3]. From the previous discussion it is clear that there was no numerical need to introduce such a viscosity, in order to stabilize the numerical scheme. Our finite-difference form of the flux terms introduces a very small second derivative term which could be looked at as an artificial viscosity. However, unlike the hydrodynamic artificial viscosity this term vanishes as $\Delta x \to 0$. In addition in all studied cases this additional term was extremely small. Furthermore, when the coordinate condition $\beta = 0$ was used these terms vanished identically.

The direct effects of an artificial viscosity on the geometry was studied by addition of the terms $\nu K_\varphi^{\varphi''}$ and $\nu K_r^{r''}$ to Eqs. (22) and (24) the evolution equations for $K_\varphi{}^\varphi$ and $K_r{}^r$. A viscosity coefficient, ν, as small as 0.05 led within 100 time steps to a 11% decrease in the C energy of the wave packet. This energy decreased further by 23% after 200 time steps.

Strong geometric artificial viscosity can serve to construct an outer layer in which waves will be dumped, without reflection. This can serve as an alternative outer boundary condition. However, in view of the success of the outgoing wave boundary condition this method was not tried in actual calculation.

V. Matter Collapse

The numerical methods which have been tested for the vacuum case are used for solution of a collapsing cylinder problems. Following the success in the vacuum case a fully constrained evolution scheme is used in most of these calculations. The coordinates (which are part of the fully constrained structure) are either isothermal ($a = b$) or "canonical", ($bc = 1$). The matter can be rotating. Then β^φ, i.e., the shift vector component in the φ direction, is introduced according to Eq. (17) so that the three metric remains diagonal. The new nonvanishing extrinsic curvature component $K_\varphi{}^r$ is evaluated from the momentum constraint equation [Eq. (25)].

The initial configurations for the collapse are static Newtonian cylinders. The metric functions have the form

$$ds^2 = (1 + 2\Phi)\, dt^2 - (1 - 2\Phi)(dr^2 + dz^2 + r^2 d\varphi^2) \tag{55}$$

for isothermal coordinates, and

$$ds^2 = (1 - 2\Phi)\, dt^2 - (1 - 2\Phi)(dr^2 + r^2 d\varphi^2) - (1 + 2\Phi)\, dz^2 \tag{56}$$

for canonical coordinates, where Φ is the Newtonian potential:

$$\Phi = \frac{1}{4r} \int_0^r \rho \tilde{r}\, d\tilde{r}. \tag{57}$$

The initial density profile is arbitrary and it is usually chosen to be Gaussian, the pressure (i.e., the internal energy) is chosen so that the configuration is in hydrostatic equilibrium. The collapse is induced by a decrease in the internal energy.

Results of such collapse are shown in Fig. 11. An outgoing pulse of C energy which begins during the bounce is clearly seen in this figure. Similar behavior is

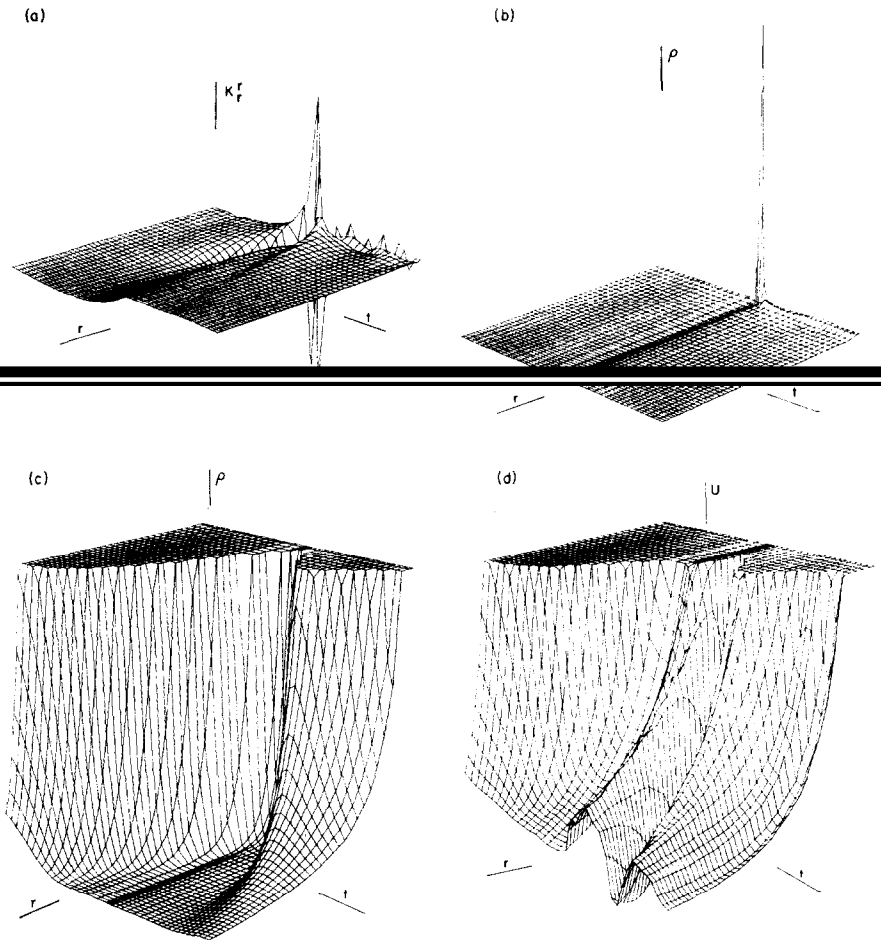

FIG. 11. The C energy density in a constrained evolution of collapsing matter cylinder using isothermal coordinates. The C energy density includes both rest mass energy density and gravitational wave energy density: (a) A typical geometric variable: $K_r{}^r$; (b) density variations; (c) the density for $\rho < 2.5 \times 10^{-4}$; (d) the C energy density for U less than 2.5×10^{-4}. Note the two (gravitational wave) pulses which do not appear on the ρ graph.

observed when the same calculations were repeated using canonical coordinates. The physical implications of these results were presented elsewhere [30, 34].

In contrast to the vacuum case in which both constrained and nonconstrained scheme performed satisfactory, only the fully constrained scheme worked well in this problem. The boundary problems which appeared in the vacuum case were enhanced, the deviation from the constraint equation diverged near the boundary, and the solution could not continued. A chopped evolution scheme had the same problem. It is not clear whether this instability is associated only with the boundary condition or it is a general feature of this scheme.

A numerical-Lagrangian scheme ($V_g = V^r$) successfully followed the collpase of the matter. However, the scheme becomes unstable when an outgoing gravitational wave emerged. The numerical grid points in the exterior region become too widely spaced and the propagation of the outgoing gravitational waves could not be traced.

VI. Cosmology

The standard Friedman metric can be written as

$$ds^2 = dT^2 - G^2(T)[dR^2/(1 - kR^2) + R^2(d\theta + \sin\theta\, d\varphi^2)]. \tag{58}$$

A Friedman Universe can also be expressed in a cylindrical coordinate. The transformation [35]

$$\frac{\partial r}{\partial R} = (1 - k\bar{R}^2)^{-1}, \tag{59}$$

$$\frac{\partial z}{\partial R} = \cos\theta(1 - k\bar{R}^2)^{-1}\,(1 - kR^2)^{-1/2}, \tag{60}$$

$$\frac{\partial z}{\partial \theta} = -\bar{R}(1 - k\bar{R}^2)^{-1}\,(1 - kR^2)^{1/2}, \tag{61}$$

where

$$\bar{R} = R\sin\theta \tag{62}$$

and

$$\frac{dT}{dt} = \alpha \tag{63}$$

reduces Eq. (58) to line element equivalent to Eq. (18) with isotropic coordinates

$$ds^2 = \alpha^2 dt^2 - G^2[(1 - k\bar{R}^2)(dr^2 + dz^2) + \bar{R}^2 d\varphi^2] \tag{64}$$

for a positive k $0 < r < r_0$, with $\bar{R}(r_0) = k^{1/2}$, while $-\infty < z < \infty$ and $0 \leqslant \varphi \leqslant 2\pi$ always.

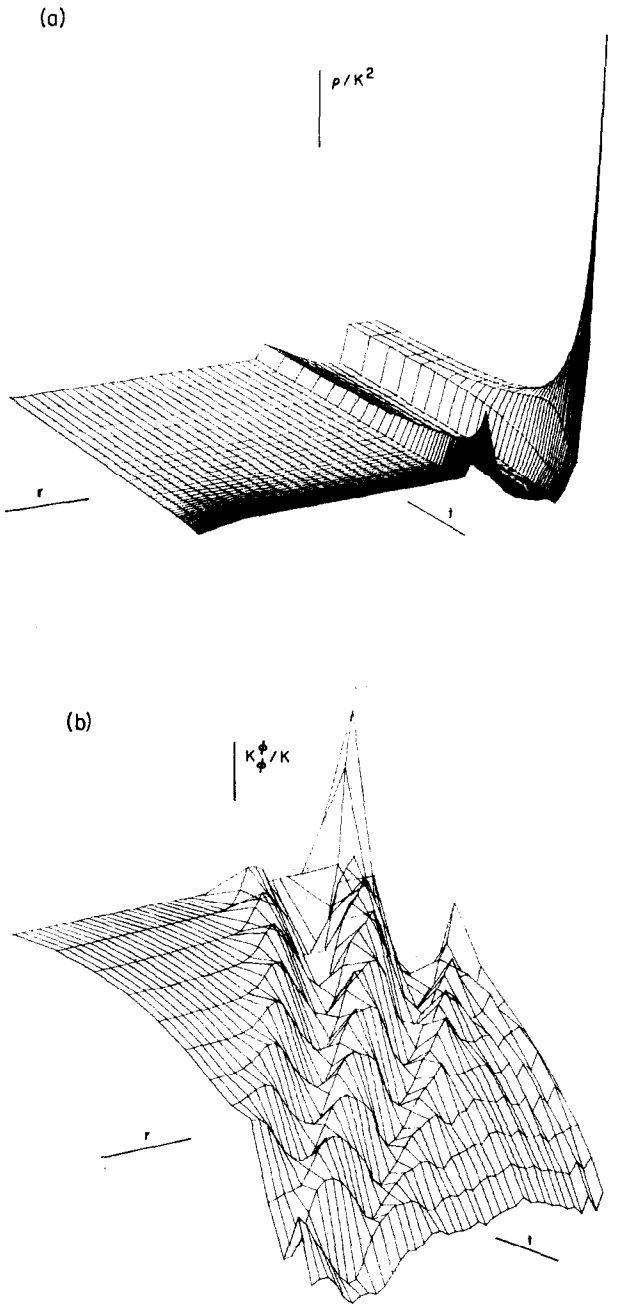

FIG. 12. Evolution of two cylindrical slices of Friedmann Universes matched together: (a) ρ/K^2; (b) propagation of an initial gravitational wave perturbation as displayed by $K_{\varphi}{}^{\varphi}/K$. Note the small amount of reflected waves from the outer boundary.

A constant t hypersurface has a constant extrinsic curvature:

$$K_r{}^r = K_z{}^z = K_\varphi{}^\varphi = \frac{1}{3}K = -\frac{\dot{G}}{\alpha G}. \tag{65}$$

Evolution of a homogeneous Friedmann Universe can be followed, trivially using the cylindrical scheme. Clearly, we are doing too much work since G which is independent of r can be calculated from a simple ordinary differential equation. Such calculation can serve to estimate the accuracy of the scheme.

While the scheme is stable for expanding solutions (an open, $k = 0$, universe was calculated accurately until the density dropped by a factor of 10^4) it becomes, not unexpectedly, unstable for a contracting solution. For example a close universe with $k = 0.1$ and initial density $\rho = 0.42$ expands until the density is $\rho = 0.16$ and contracts again. The solution is accurate to within 1 % when the contracting universe returns to its initial ($\rho = 0.43$) density. The solution is accurate within 5 % when $\rho = 2.1$, and within 20 % when $\rho = 21$, shortly before the calculation breaks down.

From a numerical point of view a solution of an expanding Universe problem was, generally, easier than the collapsing cylinder problem of the previous section. The pressure in the expanding matter falls faster than the density and after a short initial period the matter behaves like dust. There is however a new conceptual problem associated with measurement and detection of gravitational waves in a nonvacuum background.

Results of calculations of cylindrical perturbations on an expanding Friedmann Universe background are shown in Fig. 12. A constant K slicing is used in this calculation. It is interesting that while this slicing is very useful in the numerical calculation and when comparing the results with evolution of a Friedmann Universe, it imposes very strong restrictions on the initial value conditions. For example, it was impossible to find an initial constant K slice with a constant density and with a localized gravitational perturbation. Similarly, continuous matching between two Friedmann Universes was found to be possible only when the difference in k between the two solutions was small.

VII. Conclusions

The success of the numerical calculations presented here manifest the ability to achieve a very accurate numerical solution for the Einstein equations. The high precision (better than 0.5 %) in which the C energy is conserved during propagation of gravitational waves in vacuum and the very small differences between the exact (analytic) solution and results from fully constrained and partially constrained scheme serve as an excellent measure of the accuracy achieved.

There is a clear advantage to the fully constrained schemes. They contain less numerical noise and in none of the problems studied did I run into difficulties. These schemes involve a choice of a simplifying coordinate condition. It was shown that

while the main criterion in choosing the relevant coordinate conditions is the simplification of the numerical scheme, the structure of the expected final configuration should be anticipated to see if it could be expressed in a natural way in these coordinates.

The existence of an overdetermined system of equations enables us to use the deviation from the constraints as a measure of the accuracy of the solution in unconstrained or partially constrained schemes. There is no equivalent measure for a constrained solution, apart from solving the same problem using a free-evolution scheme and comparing the results. This procedure is needed to ensure that the constrained solution is not drifting from the exact one. When comparisons are made, it is found that such divergences do not occur. Another possible associated problem in a constrained scheme is propagation of signals faster than the speed of light. (This is due to the excessive usage of elliptic equations in such schemes.) This problem did not appear in any solution.

As expected a simple Lagrangian scheme failed for a collapsing cylindrical matter configuration. The coordinates (or the grid points) which followed the matter motion were not suitable for following the propagation of gravitational waves, and the scheme becomes unstable after a gravitational wave pulse was generated.

Almost all the basic problems associated with the solution of Einstein's equations are presented in these cylindrical examples. While it is not obvious that a numerical method which was successful in one-dimensional problems will be good for higher dimensions, it is clear that methods which fail in one dimension will fail in higher

ACKNOWLEDGMENTS

It is a pleasure to thank P. L. Chrzanowski, M. Cantor, B. DeWitt, P. H. Gleichauf, L. Smarr, and J. R. Wilson for many helpful discussions and the Department of Astrophysics at Oxford and the Harvard-Smithsonian Center for Astrophysics for hospitality while the manuscript was completed. The research was supported by NSF PHY77-22489.

REFERENCES

1. K. S. THORNE, in "Theoretical Principles in Astrophysics and Relativity" (N. R. Lebovitz and P. O. Vandervoort, Eds.) The University of Chicago Press, Chicago/London, 1978.
2. M. M. MAY AND R. H. WHITE, *Phys. Rev.* **141** (1966), 1232.
3. L. SMARR, *Ann. N.Y. Acad. Sci.* **302** (1977), 569.
4. K. R. EPPLEY AND L. SMARR, preprint, 1978.
5. J. R. WILSON, lecture given at GR8, Waterloo, Canada, unpublished, 1977.
6. J. R. WILSON, *in* "Proceeding of the Battelle Summer School on Sources of Gravitational Waves" (L. Smarr, Ed.), Cambridge Univ. Press, London/New York, 1979.
7. J. R. WILSON AND L. SMARR, preprint, 1978.
8. R. ARNOWITT, S. DESER, AND C. W. MISNER, *in* "Gravitation, An Introduction to Current Research," Wiley, New York, 1962.

9. A. LICHNEROWICZ, *J. Math. Pures Appl.* **23** (1944), 37.
10. N. O'MURCHADHA AND J. W. YORK, JR., *Phys. Rev. D* **10** (1974), 428.
11. N. O'MURCHADHA AND J. W. YORK, JR., *Phys. Rev. D* **10** (1974), 437.
12. J. W. YORK, JR., *in* "Proceeding of the Battelle Summer School on Sources of Gravitational Waves" (L. Smarr, Ed.), Cambridge Univ. Press, London/New York, 1979.
13. L. SMARR, *in* "Proceeding of the Battelle Summer School on Sources of Gravitational Waves" (L. Smarr, Ed.), Cambridge Univ. Press, London/New York, 1979.
14. J. R. WILSON, *Ap. J.* **173** (1972), 431.
15. P. JORDAN, J. EHLERS AND W. KUNDT, *Akad. Wiss. Abh. Math-Nat Kl. Jahrg Nr* 2 (1960).
16. A. S. KOMPANEETZ, *Zh. Eksper. Theort. Fiz.* **34** (1958), 953 (English translation: *Soviet Physics JETP* 7 (1958), 659.
17. Y. CHOQUET-BRUHAT, A. E. FISCHER, AND J. E. MARSEDEN, Lecture given at the Enrico Fermi International School of Physics, Varenna, Italy, July 1976 (to be published).
18. F. EASTABROOK, H. WAHLQUIST, S. CHRISTIANSEN, B. DEWITT, L. SMARR, AND E. TSIANG, *Phys. Rev. D* 7 (1973), 2814.
19. D. M. EARDLEY AND L. SMARR, *Phys. Rev. D*, in press.
20. C. STUMBLES, private communication, 1979.
21. F. TIPLER AND J. E. MARSDEN, preprint, 1978.
22. L. SMARR AND J. W. YORK, JR., *Phys. Rev. D* **17** (1978), 1945.
23. R. D. RICHTMYER AND K. W. MORTON, "Difference Methods for Initial-Value Problems," Intersciences, New York, 1978.
24. A. H. TAUB, *Annual Rev. Fluid Mech.* **10** (1978), 301.
25. P. L. CHRZANOWSKI AND T. PIRAN, in preparation, 1979.
26. J. P. BELLET, PhD. dissertation, University of Texas at Austin, 1978.
27. R. PENROSE, private communication, 1979.
28. S. W. HAWKING AND G. F. R. ELLIS, *in* "The Large Scale Structure of Space Time," Cambridge Univ. Press, London/New York, 1973.
29. K. S. THORNE, Ph.D. dissertation, Princeton University, 1965.
30. T. PIRAN, *in* "Proceeding of the Battelle Summer School on Sources of Gravitational Waves" (L. Smarr, Ed.), Cambridge Univ. Press, London/New York, 1979.
31. A. EINSTEIN AND N. ROSEN, *J. Franklin Inst.* **223** (1937), 43.
32. C. W. MISNER, K. S. THORNE, AND J. A. WHEELER, "Gravitation," Freeman, San Francisco, 1973.
33. J. CENTRELLA, Ph.D. thesis, Cambridge University, 1978.
34. T. PIRAN, *Phys. Rev. Lett.* **41** (1978), 1085.
35. W. J. COCKE, *J. Mathematical Phys.* 7 (1966), 1171.
36. B. SHUTZ, Lecture Notes in Physics, Vol. 14, Springer-Verlag, Berlin/New York, 1972.
37. K. R. EPPLEY, Ph.D. thesis, Princeton University, 1975.
38. F. J. FLAHERTY AND D. BRILL, *Ann. Inst. H. Poincaré* **28** (1978), 335.
39. K. R. EPPLEY, *in* "Proceeding of the Battele Summer School on Sources of Gravitational Waves" (L. Smarr, Ed.), Cambridge Univ. Press, London/New York, 1979.
40. B. DEWITT, private communication, 1977.
41. L. SMARR, Ph.D. thesis, University of Texas at Austin, 1975.
42. L. SMARR AND J. W. YORK, JR., *Phys. Rev. D* **17** (1978), 2529.
43. J. W. YORK, JR., *Phys. Rev. Lett.* **28** (1972), 1982.